Proc. 1995 IEEE Int. Conf. Robotics and Automation.
Nagoya, Japan. pp. 2305--2310.

Design of Shape Memory Alloy Actuator with High Strain and Variable Structure Control

Danny Grant Vincent Hayward

Department of Electrical Engineering and
Research Centre for Intelligent Machines
McGill University
Montréal, Québec, H3A 2A7, Canada
grant@cim.mcgill.ca, hayward@cim.mcgill.ca

Abstract

A novel Shape Memory Alloy (SMA) actuator consisting of a number of thin NiTi fibers woven in a counter rotating helical pattern around supporting disks is first described. This structure can be viewed as a parallel mechanism used to accomplish a highly efficient transformation between force and displacement. The actuator overcomes the main mechanical drawback of shape memory alloys, that being limited strain. Two variable structure controllers are applied to a pair of antagonist actuators. The first involves a switching control input creating a sliding mode in conjunction with a linear control activated within a boundary layer in the vicinity of the set point. The second involves a multi-stage switching control that simplifies amplifier construction. Experimental performance results in the time domain are discussed.

1 Introduction

With the continued miniaturization of robotic systems comes the need for powerful, compact, lightweight actuators. Conventional techniques such as electric, hydraulic, and pneumatic actuators, suffer from a drastic reduction of the amount of power they can deliver as they scale down in size and weight. [7] To overcome this limitation, different actuator technologies have been investigated, in particular Shape Memory Alloys (SMA). Shape Memory Alloys have a high strength to weight ratio which makes them ideal for miniature applications. A SMA fiber can achieve a maximum pulling force of 180 MPa. Comparing this to an electro-magnetic actuator, which can only achieve .002 MPa, this represents an almost 10^5 increase in strength per cross sectional area. Thin fibers of shape memory alloy can accomplish actuation by being pretreated to contract upon heating. The contraction is a result of the fiber undergoing a phase transition between its Martensitic and Austenitic phases. When in the cool phase (martensitic) the alloy is malleable and can easily be deformed by applying external stress. The original pretrained shape can then be recovered by simply heating the fiber above its phase transition temperature. Since the alloy is resistive it can easily be heated electrically.

Along with SMA's high strength to weight ratio comes several limitations. SMA's possess highly nonlinear properties [1], such as a complicated hysteresis loop in the transition temperature relationship. They can however still be controlled through the use of feedback and other control techniques, and a variable structure controller will be applied in the second part of this paper. The main physical limitation that needs to be overcome is the absolute percent strain. SMA's can achieve a workable strain of 5 percent.

Many of the designs of actuators using shape memory alloys depend on mechanically amplifying the displacement either through the use of long straight fibers [5], [9], [12], or through the use of coils [6], [7], [9]. The proposed actuator achieves mechanical motion amplification that is more compact than a long straight length of fiber, and more efficient than using coils.

2 Shape Memory Alloy Actuator

The actuator, shown in Figure 1, consists of twelve thin NiTi fibers woven in a counter rotating helical pattern around supporting disks. The disks are sepa-

IEEE International Conference
on Robotics and Automation
0-7803-1965-6/95 $4.00 ©1995 IEEE

rated by preloading springs that keep the fibers under tension when relaxed. When the fibers are heated, they contract pulling the disks together.

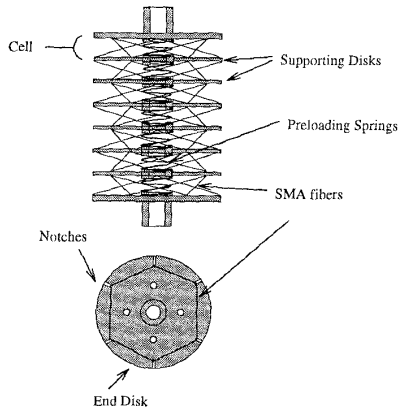

Figure 1: Shape memory alloy actuator

The weave pattern of the fibers accomplishes a displacement amplification. Essentially the abundant force of the alloy is being traded off for a displacement gain. This transformation between force and displacement is highly efficient since the only loss in work is due to the slight bending of the fibers. Unlike shape memory alloy coils, the entire cross section of the fiber in the weave is performing work in the contraction. Coils suffer from the debilitating drawback of requiring a larger diameter than necessary. This is especially negative, since the response time is directly related to fiber diameter. The response of the actuator is limited by the cooling rate of the NiTi fibers, which directly depends on the fiber's surface area to volume ratio. The higher this ratio the more rapidly the fiber will cool. A great deal of the material is wasted in SMA coils since, during the shape memory effect, only the skin of the coil is actually contracting at the maximum amount. The internal diameter of the coil is acting both as a heat sink and as a source of opposing force to the desired motion.

The weave pattern also results in an ideal 'tensegrity' structure [3], with all compression members being passive and all tension members active, resulting in an optimal use of the material.

2.1 Simplified Case

The kinematic amplification can best be seen by considering the simplified case consisting of two beams and two fibers as shown in Figure 2.

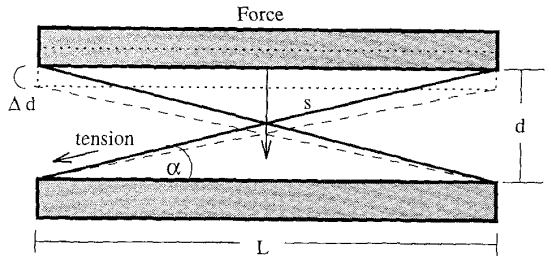

Figure 2: Simplified case:Two beams with two fibers

As the two fibers contract, the two beams are pulled together. The displacement gain, $\Delta d/\Delta s$, is defined as the change in stroke along the separating distance, divided by the change in the fiber length. Since ideally the motion is constrained along d the instantaneous displacement gain is given by:

$$\frac{\delta d}{\delta s} = \frac{s}{\sqrt{s^2 - L^2}} = \frac{1}{\sqrt{1 - cos\alpha^2}} = \frac{1}{sin\alpha} \qquad (1)$$

The displacement gain is inversely proportional to the sine of the weave pitch. As the disks get closer together the displacement gain dramatically increases, asymptotically approaching infinity.

2.2 SMA actuator

The weave pattern of the SMA actuator achieves a kinematic amplification for each cell of the actuator. All the radial components of the tension forces of the twelve fibers cancel, leaving only a common axial stress force component. In this manner the displacement gain overcomes the main mechanical drawback of the SMA, while the force attenuation is compensated by using several fibers in parallel. The actuator is no longer limited to the absolute percent strain of the fiber. The displacement gain also allows the fiber to operate at reduced percent absolute strain, and since the cycle lifetime of the SMA fibers increases dramatically when they operate at a lower than absolute strain, the cycle lifetime can also be increased. To obtain a reasonable response, 100 μm diameter SMA fibers were chosen for the actuator prototype. Twelve 100 μm fibers acting in parallel, allow rapid cooling in ambient air without compromising strength.

3 Design Parameters

The prototype represents only one configuration of the SMA actuator's parameters [4]. The supporting disk size and spacing, the number of fibers, and the displacement gain are all adjustable parameters. Figure 3 will define the variables involved, highlighting only one of the fibers in a single actuator cell.

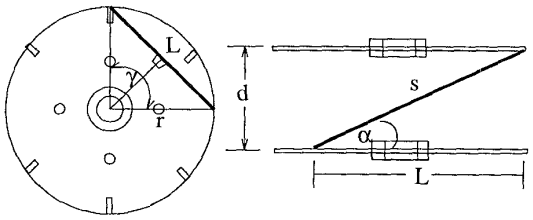

L - length of fiber along disk
r - disk radius
γ - offset angle between succesive disks
s - length of fiber
d - interdisk seperation
α - weave pitch angle

Figure 3: Variables involved

All the parameters are inter-related leading to an engineering problem for which an acceptable trade-off must be found within set constraints. Equation(1) shows that the displacement gain is inversely proportional to the sine of the weave pitch. The weave pitch in turn is dependent on the fiber weave pattern and the radius and spacing of the supporting disks. The weave pattern is determined by the number of notches around the disk, and the relative alignment of successive disks.

The offset angle, γ, is the angle between notches of successive disks in the actuator. For the actuator prototype in Figure 1, eight disks were chosen with 6 notches spaced 60^o apart. The prototype actuator was constructed by aligning the disks vertically so that each successive disk was offset by 30^o. The weave pattern was obtained by threading a single fiber along the notches of the eight disks. Adjacent disks were connected by the fiber through notches that were separated by an offset angle of 90^o. The two end disks are woven along successive notches as shown in Figure 1. To get a better idea of how the fibers are woven, imagine the support disks of the actuator rolled out so that they are flat. Figure 4 shows a four disk actuator with the disks unraveled. The fiber weave would begin at an end disk and pass through the successive points one through five.

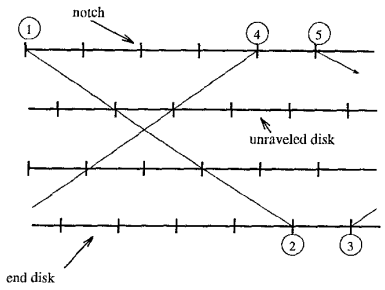

Figure 4: Unraveled fiber weave

The fiber would then continue going back and forth between the two end disks until it arrived back at its starting position. In this manner it is possible to manually connect many fibers in parallel, simply and securely using a small jig in a manner of minutes. After the weave was completed the two ends of the fiber were merely tied in a knot. This also provided a secure mechanical connection as most of the stress on the fiber occurs at the notches. The final result is twelve fibers woven in counter helical rotations such that all radial forces cancel out upon contraction.

3.1 Displacement Gain

The displacement gain can be increased by increasing the offset angle,γ or by decreasing the inter-disk distance d. There are of course limits on both of these parameters. As the offset angle approaches 180 degrees, the fibers approach the center of the disk. This causes the structure to become more unstable and reduces the available space in the center for the placement of the springs and/or a position sensor. The radius of the inner bounding cylinder, shown in Figure 5 can be found by trigonometry to be $r_i = r * \cos\gamma$ where r is the disk radius and γ is the offset angle

Decreasing the distance in between the disks dramatically increases the displacement gain but limits the amount of stroke per cell. If the disks begin very close together they can only move a small distance before they come in contact with one another.

The force generated by the actuator can be adjusted by choosing the number and size of fibers used in the weave. Obviously the more fibers that are acting in parallel the larger the force generated. Again there is a limitation here on the number of fibers that can be used. As the number of fibers increases so does the

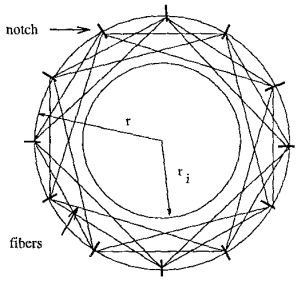

Figure 5: Inner bounding cylinder

fiber interference in the weave. Fibers with a larger diameter can be chosen, but at the expense of response as cooling times will increase. The actuator is completely modular in the sense that any number of cells can be cascaded together.

4 Experimental Setup

The fibers used in the actuator only exhibit the one way shape memory effect. For this reason it is necessary to force bias individual actuators so that they will return to their original length when cooled. This can easily be accomplished by using biasing springs or by using actuators in an antagonistic fashion. Shape memory alloys are especially suited to antagonistic arrangements since the force required to deform the alloy is much less than the force generated by the phase transformation. Using the actuators in an antagonistic fashion also results in improved system response. The response time of the actuator system will then strongly depend on heat activation, which can be tuned according to the input current amplitude. For these reasons open loop experiments were performed using two actuators in an antagonistic fashion as shown in Figure 6.

4.1 Open Loop Response

The time domain open loop response to a step of input current applied to the actuator can be seen in Figure 7. The left side of Figure 7 shows the results of heating one of the actuators with a 50 ms pulse while varying the current amplitude by .5 A steps from 8.0 A to 14.5 A. Note that the twelve fibers are electrically connected in parallel, hence the current in each fiber is divided by a factor of twelve.

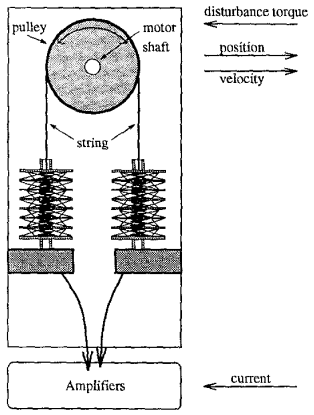

Figure 6: Top view of testbed

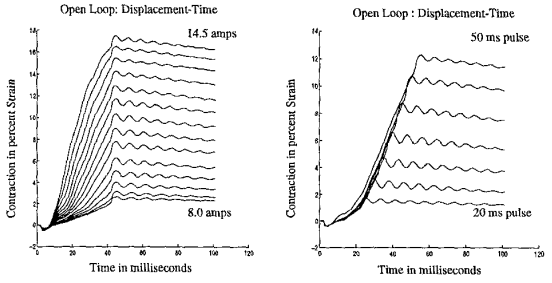

Figure 7: Open loop response

The right side of Figure 7 shows the results of heating the actuator with a constant current of 8.0 A and varying the duration of the pulse between 20 ms and 50 ms. There are four main observations to be made about theses curves.

The open loop step response of the actuator reveals that although the phase transformations exhibit highly non-linear properties, a markedly linear relationship between heating time and percent strain can be observed in a large portion of the graph. This relationship occurs after the alloy's temperature reaches M_s, the martensite starting temperature. Before that temperature is reached, the fiber undergoes thermal expansion which explains why the response appears to be "in the wrong direction" when heating is applied to a fiber significantly colder than M_s. This effect could be approximated as a time delay, but can be ignored since when the actuator is under control for normal operation its temperature is kept in the vicinity of

M_s.

The slope of the line depends monotonically on the magnitude of the current pulse used to heat the fiber. The higher the current the faster the temperature increase and therefore the faster the response. Again, the relationship between current magnitude and strain rate of change is quasi-linear.

Considering in turn pulse time as a control signal, it is seen that the amount of displacement is in direct relationship with pulse duration and also in a monotonic quasi-linear relationship as exhibited by the final values of the family of curves.

The oscillatory behavior superimposed on the response or ringing, is due to the linear under-damped second-order dynamics of the system accounting for load inertia, fiber elasticity and actuator damping. In the controller design, this effect has been ignored since it will be designed to track position and consequently will stiffen the system by a large factor. Under the simple controllers about to be described all ringing is eliminated for a large range of the load inertial parameters.

4.2 Controller Design

A considerable amount of work has been concerned with the modeling of shape memory alloy actuators [2], [8], [11], while relatively less attention has been paid to the design of feedback control laws. Many feedback control techniques reported in the literature applied to shape memory actuators are in fact linear compensators such as P, PD or PID controllers [11], [12], or close cousins.

The dynamics of shape memory actuators are predominantly nonlinear because the energy conversion principle, from heat to mechanical, relies on exploiting phase transitions in a metal, creating at least significant hysteresis in addition to many other nonlinear effects having memory or not. In addition, the detailed properties of the dynamics of shape memory alloys vary greatly with their metallurgy, fabrication process, training techniques [6], aging, ambient conditions, and thus are difficult to describe accurately and in general terms. Moreover, most of the detailed descriptions of their underlying physics are often not very useful for controller design.

The overwhelming advantage of variable structure control is that relatively few parameters representing the knowledge of the physical properties of the plant need to be known since only inequality conditions need to be satisfied in the design [13]. It is also well known that variable structure control is quite insensitive to plant parameter variations since the resulting trajectory resembles a time near-optimal switching curve.

It is often stated that a disadvantage of variable structure control is the discontinuous nature of the control signal which may cause problems in actuators in terms of ringing, excessive dissipation, and excitation of unwanted dynamics in the plant being driven by these actuators. These problems sometimes can be solved by the introduction of smooth switching laws while retaining some of the advantages of the technique. Another approach is the introduction of boundary layers in the vicinity of the so-called sliding surfaces when the nature of the plant precludes the switching frequency to approach infinity, see for example [10].

For some actuation techniques, switching is not a problem and clearly shape memory alloy actuation is one of them: the mechanical energy is derived from heat which makes the actuators naturally low pass and thus undisturbed by step or impulse inputs. Moreover, the robustness properties of variable structure control combined with the modeling difficulties of shape memory alloy actuators creates considerable incentive to apply the former to the later. There is also yet another reason which makes this combination attractive.

One original motivation for variable structure control is exceedingly practical [13]. No amplifiers, valves, or other continuous energy throttling mechanisms are needed, only switches. As previously mentioned, one great attraction of shape memory allow actuators is the possibility for miniaturization. With variable structure control, the energy throttling device can be as simple as a single FET switching current on and off from a power bus, thereby opening a path toward a mechatronic-type high degree of integration, including in one single unit actuation, sensing, control and energy throttling.

4.3 Two Stage - Linear controller

Figure 8 shows a block diagram of the initial two stage linear controller applied to the actuator. If the error is large then the maximum constant feedback is used. As the state trajectory approaches the set point the control is switched to the linear proportional controller.

This results in a smoother motion as the state trajectory slows down as it approaches the set point switching surface. The disadvantage of this, is that in the vicinity of the set point the feedback signal is low, so the plant is easily disturbed by small perturbations.

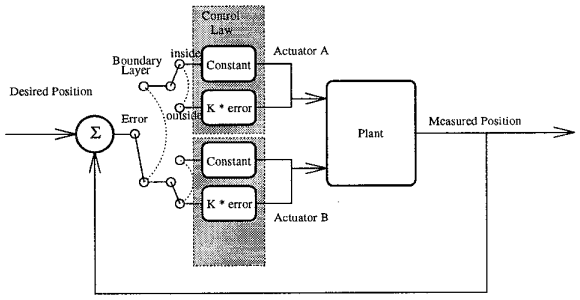

Figure 8: Block diagram of two stage controller

The adjustable parameters for the two stage linear controller are: 1) location of the boundary layer; 2) the amplitude of the constant current pulse; and 3) the gain of the linear proportional controller.

4.4 Two Stage - Constant Magnitude

The two stage constant magnitude controller is identical to the two stage linear controller except now a smaller constant input is used near the set point switching surface. This eliminates the need for a proportional amplifier to realize the control gain near the switching surface, simplifying the amplifier construction. The controller should also be better able to resist perturbations as a significant control gain is applied for even a slight perturbation.

A good value for this gain near the set point is the current level needed to maintain the current temperature of the actuator. That is a current that will provide enough heat to compensate for the ambient heat loss.

5 Experimental Results

5.1 Two Stage - Linear Boundary Layer

Figure 9 shows the step and ramp responses of the two stage linear controller with the parameters set as follows: 1) maximum gain = 6 A; 2) linear proportional gain = 16.37 * error in A; 3) boundary layer = .25 mm. The various parameters have been tuned for the specific input step.

The step response, although smooth, never reaches the set point, and has a steady state error of 0.14 mm. Switching between the two actuators does not take place here since the plant's trajectory never reaches the sliding surface. The rise time, measured from the 10% to the 90% of the final value is, 87 ms with a 50 ms delay.

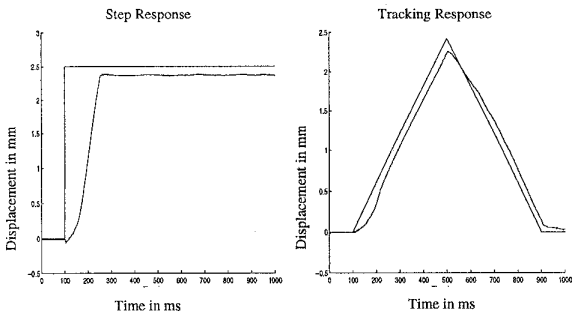

Figure 9: Step and ramp response of two stage linear controller

The tracking response has a time lag of 36 ms due to the delay between applied current and the phase transition. Also note that the slight dip at the beginning of the ramp response is due to the fact that the actuator responds at a lower rate at the beginning of the phase transition as can also be seen in the open loop step response of Figure 7.

5.2 Two Stage - Constant Magnitude

Figure 10 shows the step and ramp response to the two stage constant controller with the parameters set as follows: 1) maximum gain = 6 A; 2) gain near set point = 4 A 3) boundary layer = .25 mm.

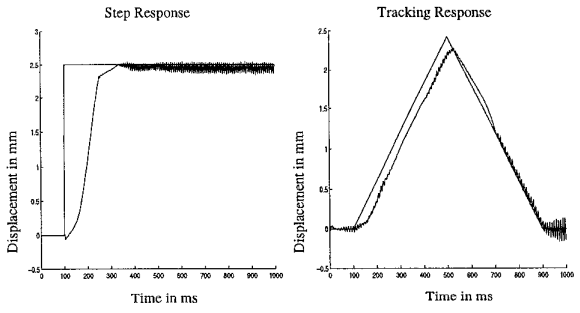

Figure 10: Step and ramp response of two stage constant magnitude controller

The step response here enters a limit cycle of 116 Hz with an average value steady state error of .04 mm. The existence of a limit cycle, as a consequence of the

type of control applied, is seen here as a benefit rather then a problem. It is well known that the application of a high frequency periodic signal (ie. dithering) to a non-linear plant, having in particular hysteresis, yields a system that is linearized for small signals and which has reduced steady state error.

The rise time is 91 ms. The tracking response has a time delay of 28 ms for the positive slope and is nearly zero for the negative slope. This discrepancy in tracking is a byproduct of the displacement gain. As the actuator contracts the displacement gain increases as the weave pitch angle is decreasing. When the actuator is extended it has a lower displacement gain then when it is contracted. This is primarily why the two above controllers can only be ideally tuned for a single step response. As a refinement to the two stage constant magnitude controller, a different magnitude pulse was used inside the boundary layer depending on the state space information whether the actuator was extended or contracted. Again in an effort to keep the controller as simple as possible, a single magnitude was chosen for the feedback inside the boundary layer. The switching scheme is then given as in Figure 11, and the results of such a controller can be seen in the series of steps shown on the left in Figure 12.

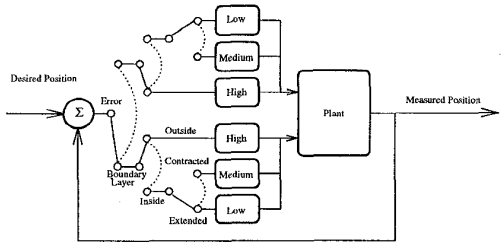

Figure 11: Block diagram of refined controller

Ideally the constant magnitude pulse inside the boundary layer should have an amplitude that compensates for the displacement force tradeoff throughout the workspace of the actuator. On the left of Figure 12 the results of using only two magnitude pulses inside the boundary layer can be seen. For small steps (.5 mm) the limit cycle is slightly higher than the set point. The magnitude of the medium pulse is too high compared to the magnitude of the low pulse. However for large steps (2.5 mm) the limit cycle is slightly below the set point. The magnitude of the medium pulse is too small compared to the low pulse. And of course for the medium steps the limit cycle is nearly centered around the set point.

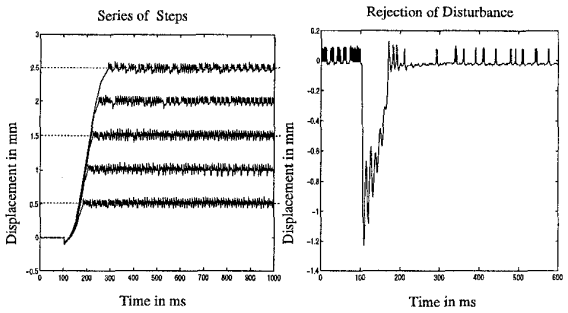

Figure 12: left) Series of steps; right) Disturbance rejection

5.3 Disturbance Rejection

By construction of the set point switching surface, any deviance from the set point results in an immediate gain that drives the plant back to the set point surface. On the right of Figure 12 a disturbance torque step of .03 Nm is applied by the testbed at 100 ms. This corresponds to 1.0 N at the actuator or 25% of the actuator's maximum force.

6 Conclusions

A novel actuator using shape memory alloys has been proposed that overcomes the main drawback of shape memory alloys, that being limited strain. The abundant force available with SMA fibers is efficiently transformed to increase displacement by weaving fibers around supporting disks. An actuator prototype, see Figure 13 has been constructed with the following properties:

- light weight - 6 grams,
- compact - 17 mm cylinder x 30 mm long,
- powerful - 4 newtons,
- direct drive actuator,
- requires no gears or lubrication,
- smooth movements,
- silent and
- modular.

Open loop experiments have been conducted to demonstrate the intrinsic properties of the SMA actuator.

Two stage switching control laws were applied to the shape memory alloy actuator. The controller is

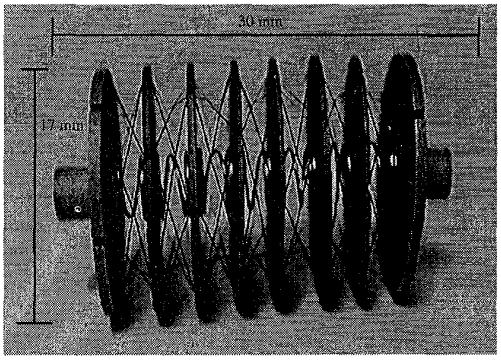

Figure 13: SMA actuator prototype

based on a simple concept and produces satisfactory results. By adjusting the control gains it is possible to reach a set point with a small steady state error or to go into a desirable limit cycle within a specified limit.

The two stage constant controller further demonstrated that the added complexity of a linear proportional controller is not required. Similar results can be obtained with the two stage constant magnitude controller which can be implemented in practice with very few electronic components. Further research has been done on implementing this technology for a compact pan, tilt, and torsion camera unit [4].

Acknowledgments The support of Prof. Martin D. Levine was essential to the completion of this project. The research was mostly funded by IRIS, the Institute for Robotics and Intelligent Systems part of Canada's National Centers of Excellence program (NCE), under the heading "Orienting Devices for Dynamic Vision". Additional funding was provided by a team grant from FCAR, le Fond pour les Chercheurs et l'Aide à la Recherche, Québec, and an operating grant from NSERC, the National Science and Engineering Council of Canada.

References

[1] T.W Duerig, K.N. Melton, D. Stockel, and C.M. Wayman. *Engineering Aspects of Shape Memory Alloys.* Butterworth-Heinemann Ltd, Toronto, 1990.

[2] D.Yang, G.Lin, and R.Warrington. A computational model of shape memory alloys for the design and control of micro-actuators. *Micromechanical Systems,* v4, 1992.

[3] Buckminster Fuller. *Inventions: The Patented Work of Buckminster Fuller.* St. Martin's Press, Toronto, 1983.

[4] D. Grant. Shape memory alloy actuator with an application to a robotic eye. Master's thesis, McGill University, 1995.

[5] M. Hashimoto, Mansanori Takeda, Hirofumi Sagawa, and Ichiro Chiba. Application of shape memory alloy to robotic actuators. *Journal of Robotic Systems,* 2(1):3–25, 1985.

[6] I. Hunter, S. Lafontaine, J. Hollerbach, and P. Hunter. Fast reversible NiTi fibers for use in microrobotics. In *Microelectro-mechanical Systems,* Nara,Japan, Jan 1991.

[7] K. Ikuta. Micro/miniature shape memory alloy actuator. In *IEEE Robotics and Automation Society,* volume 3, pages 2156–2161, Los Alamitos, California, May 1990. IEEE Computer Society Press.

[8] K. Ikuta, M. Tsukamoto, and S. Hirose. Mathematical model and experimental verification of shape memory alloy for designing micro actuator. In *Proc. of the IEEE MicroElectroMechanical Systems Conference,* pages 103–108, 1991.

[9] K. Kuribayashi. A new actuator of a joint mechanism using TiNi alloy wire. *The Int. Journal of Robotics Research,* 4(4), 1986.

[10] W. Li and J-J. E. Slotine. *Applied Non-Linear Control.* Prentice Hall, 1991.

[11] D. R. Madill. Modelling and stability of a shape memory alloy position control system. Master's thesis, Applied Science, University of Waterloo, 1993.

[12] D. Reynaerts and H. Van Brussel. Development of a SMA high performance robotic actuator. In *Fifth International Conference on Advanced Robotics,* volume 2, pages 19–27, New York, NY, 1991.

[13] V. L. Utkin. *Sliding Modes in Control Optimization.* Springer-Verlag, 1992.